Wind and Structures, Vol. 1, No. 2 (1998) 127-144
DOI: http://dx.doi.org/10.12989/was.1998.1.2.127

Numerical study of wake structure behind a square cylinder at high Reynolds number

Sungsu Lee†

Cooperative Institute for Research in Environmental Sciences, University of Colorado/NOAA, CO, 80303, U.S.A.

Abstract. In this paper, the wake structures behind a square cylinder at the Reynolds number of 22,000 are simulated using the large eddy simulation, and the main features of the wake structure associated with unsteady vortex-shedding are investigated. The Smagorinsky model is used for parametrization of the subgrid scales. The finite element method with isoparametric linear elements is employed in the computations. Unsteady computations are performed using the explicit method with streamline upwind scheme for the advection term. The time integration incorporates a subcycling strategy. No-slip condition is enforced on the wall surface. A comparative study between two-and three-dimensional computations puts a stress on the three-dimensional effects in turbulent flow simulations. Simulated three-dimensional wake structures are compared with numerical and experimental results reported by other researchers. The results include time-averaged, phase-averaged flow fields and numerically visualized vortex-shedding pattern using streaklines. The results show that dynamics of the vortex-shedding phenomenon are numerically well reproduced using the present method of finite element implementation of large eddy simulation.

Key words: large eddy simulation; vortex shedding; finite element method.

1. Introduction

Many engineering problems related to bluff bodies are frequently associated with flow-structure interactions. It is of particular importance when slender structures such as high-rise buildings or long-span bridges are considered. Decks of long-span bridges are especially susceptible to the flow-structure interactions, including aeroelastic effects associated with vortex-induced oscillation, flutter, galloping and buffeting. Hence, understanding of vortex-shedding phenomenon and fluid-structure interaction is of practical interest in engineering applications. In order to investigate the flow field around such structures, the present study conducts numerical computations of unsteady flows around a square cylinder which has sharp corners.

Earlier studies of computations and experiments show that a flow field around a square cylinder at low Reynolds number remains two-dimensional and laminar and the flow reveals nearly sinusoidal patter with a unique (vortex-shedding) frequency. As the Reynolds number increases, the three-dimensional (stochastic) perturbation due to turbulence becomes more significant. Franke (1990) and Lee (1998) numerically showed that stochastic effects emerge at the Reynolds number of 250, resulting a subhamonic fluctuation of the forces acting on the cylinder in addition to a primary frequency associated with the Strouhal number.

† Research Associate

Increase in the Reynolds number results in broad energy spectra of the unsteady, three-dimensional flow fields. This requires a large number of grid points for direct numerical simulation (DNS) to be considered. However, a practical application of DNS to engineering problems are not feasible even with recent development of computing facilities. Instead, turbulent flow simulations, using the Reynolds-averaged Navier-Stokes equations (RANS) with κ-ε model and more recently the large eddy simulation (LES), have been carried out by many numerical studies. In wind engineering points of view, LES was first brought into attention by a study of Murakami (1987).

As for numerical methods, most of earlier LES studies employed finite difference or finite volume method. However, they revealed an ambiguous definition of wall boundary at the sharp corners when staggered grids are used, Yu (1996). In order to avoid the ambiguity, the present study employs finite element method (FEM) which was used for LES by Lee (1998, 1997). There have been only a few reported studies in which FEM was implemented for LES, including Nomura (1995).

The aim of this paper is to apply a finite element implemented LES to calculation of high Reynolds number vortex-shedding flows. Galerkin FEM (GFEM) and the conventional Smagorinsky (1963) SGS model are employed. The present paper first presents a comparative study between two-and three-dimensional computations to assess the importance of the three-dimensionality in simulating turbulent flow. Next described are the simulated three-dimensional wake structures around a square cylinder at Re=22,000. The presented results include mean and root-mean-square (RMS) of the velocity fields, compared with available experimental and computational data published by other researchers.

2. Background

2.1. Formulation of large eddy simulation

A rationale of LES lies in decomposition of flow variables into resolvable scales (RS) and small scales (SGS), which is accomplished by spatial filtering. An instantaneous variable $u(\vec{x}, t)$ is described as

$$u = \bar{u}(\vec{x}, t) + u'(\vec{x}, t) \tag{1}$$

where $\bar{u}$ and u' are RS and SGS, respectively. The filtered value (RS) are obtained by

$$\bar{u}_i(\vec{x}, t) = \int_\Omega G(\vec{x} - \vec{\xi}; \Delta) u_i(\vec{\xi}, t) d\vec{\xi} \tag{2}$$

where G is a filter function, and Δ is filter size which determines the cutoff scale of spatially fluctuating variables. The present study employs box-type filter defined by

$$G(r) = \frac{1}{\Delta} \quad \text{for} \quad r \leq \frac{\Delta}{2}, \quad = 0 \quad \text{for} \quad r > \frac{\Delta}{2} \tag{3}$$

Applying the filtering operation defined by Eq. (2) to the Navier-Stokes equations (NSEs) leads to

$$\frac{\partial \bar{u}_i}{\partial t} + \bar{u}_j \frac{\partial \bar{u}_i}{\partial x_j} = -\frac{1}{\rho} \frac{\partial \bar{p}}{\partial x_i} + \nu \frac{\partial \bar{S}_{ij}}{\partial x_j} - \frac{\partial \tau^*_{ij}}{\partial x_j} \tag{4}$$

where ν is the kinematic viscosity of the fluid, $\bar{p}$ is the filtered pressure,

$$\bar{S}_{ij} = \frac{1}{2}\left(\frac{\partial \bar{u}_i}{\partial x_j} + \frac{\partial \bar{u}_j}{\partial x_i} \right) \tag{5}$$

and

$$\tau^*_{ij} = \bar{u}_i \bar{u}_j - \bar{u}_i \bar{u}_j \tag{6}$$

Similar to RANS formulation, the last term of the right hand side of Eq. (4) is called Reynolds SGS stress which requires phenomenological turbulent models. Another frequently referred form of the momentum equations is

$$\frac{\partial \bar{u}_i}{\partial t} + \bar{u}_j \frac{\partial \bar{u}_i}{\partial x_j} = -\frac{1}{\rho} \frac{\partial P}{\partial x_i} + \nu \frac{\partial \bar{S}_{ij}}{\partial x_j} - \frac{\partial \hat{\tau}_{ij}}{\partial x_j} \tag{7}$$

where

$$\hat{\tau}_{ij} = \tau^*_{ij} - \frac{1}{3}\delta_{ij}\tau^*_{kk}$$

and

$$P = \bar{p} + \frac{1}{3}\tau^*_{kk} \tag{8}$$

Most popular approach employed in SGS modeling of LES has been the Smagorinsky model which is based on the eddy viscosity concept and the mixing length theory. Even if the Smagorinsky model has drawbacks including overestimation of eddy viscosity near solid walls, it has been popular due to its simplicity and ability to predict global energy transfer. The overestimation of the eddy viscosity can be artificially suppressed using damping function such as Van Driest function. However, the present study did not include this modification. The eddy viscosity concept leads to the following model :

$$\hat{\tau}_{ij} = -2\nu_{SGS}\bar{S}_{ij}. \tag{9}$$

where ν_{SGS} is the eddy viscosity for LES which has the form of

$$\nu_{SGS} = (C_S \Delta)^2 \sqrt{2\bar{S}_{ij}\bar{S}_{ij}} \tag{10}$$

where C_S is the Smagorinsky constant. In the present computations, it is set to 0.15 and 0.1 for 2D and 3D cases, respectively.

The momentum equations Eq. (7) and the continuity equation are nondimensionalized using the length of a side of the square cylinder, H and the inflow velocity U_O as the reference length and

velocity scales, respectively. The Reynolds number and the Strouhal number are thus defined as HU_O/v and fH/U_O, where f is the vortex shedding frequency. Time and pressure are non-dimensionalized using H/U_O and ρU_O^2, respectively.

2.2. Numerical scheme

The governing equations given above are approximated using the spatial discretization by GFEM with isoparametric elements. Quadrilateral (2D) or brick (3D) elements with constant pressure and linear interpolation functions for velocity field are employed. The resulting algebraic equations are

$$\boldsymbol{M}\dot{\boldsymbol{V}}+\boldsymbol{K}(\boldsymbol{V})\boldsymbol{V}-\boldsymbol{C}\boldsymbol{P}=\boldsymbol{Q} \tag{11}$$

and

$$\boldsymbol{C}^T\boldsymbol{V}=\boldsymbol{0} \tag{12}$$

where $\boldsymbol{V}$ is a global vector containing the nodal values of the velocity field, $\boldsymbol{P}$ is a global pressure vector, and $\boldsymbol{Q}$ is a force vector incorporating the velocity natural boundary conditions. $\boldsymbol{M}$ is the mass matrix and $\boldsymbol{K}$ contains the advection and the diffusion terms. $\boldsymbol{C}$ is the gradient matrix while its transpose, $\boldsymbol{C}^T$ is the divergence matrix. The Reynolds SGS stress term is included in $\boldsymbol{K}$ and the eddy viscosity v_{SGS} is evaluated at the centroid of each element, at each time step.

Time integration is performed using the explicit (Euler) method in which a Poisson equation is solved for the pressure field at each time step, by a conjugate gradient method, to ensure that the flow field is divergence free. The Euler method is modified to incorporate a subcycling strategy which permits less frequent updates of the pressure field, with a little loss in accuracy. The cost-effectiveness of this scheme was demonstrated by Gresho (1984). A streamline upwind scheme, Brooks and Hughes (1982), for the stability of the explicit time integration and the minimization of the crosswind diffusion, is used for the nonlinear advection. The initial flow field is set to zero except for the inflow boundary, and it is next modified to satisfy the continuity equation by solving an auxiliary Poisson equation.

Fig. 1 depicts the schematic diagram of the sectional view of the computational domain employed in this study. No-slip condition is enforced on the surface of the solid wall. Inflow

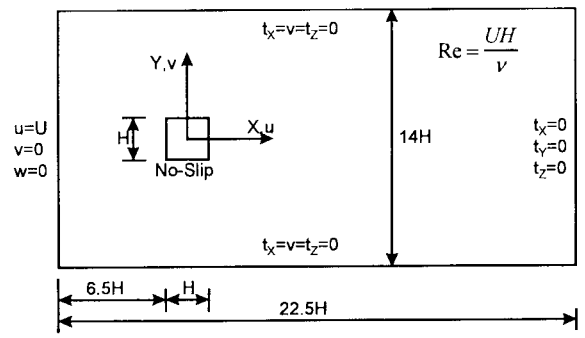

Fig. 1 Computational domain and boundary condition

has uniform velocity, and traction free condition is imposed on the outflow boundary. On upper and lower boundaries, traction free conditions are imposed on only horizontal components where vertical velocity is set to zero. The 3D computation employs the spanwise length of the cylinder of 2H, with the periodic boundary condition imposed.

3. Comparison between 2D and 3D computations

As Roshko (1993) pointed out, the 3D effects are one of the most problematic aspects of bluff body aerodynamics, especially at high Reynolds numbers. In order to assess the effcets of the three dimensionality in simulation of high Reynolds number flow, both 2D and 3D computations are carried out.

The number of elements employed in the 2D computation is 4776 elements depicted in Fig. 2. The characteristic length of the smallest grid adjacent to the cylinder surface is 0.01H. In the case of 3D simulation, uniformly distributed 10 elements are employed in the spanwise direction, resulting in the total number of 47760 elements. Since detailed measurements of the wake structures behind a square cylinder at Re=22,000 was conducted by Lyn (1989, 1994, 1995) using laser doppler velocimetry, the flow at Re=22,000 has been a benchmark case for the computational studies by many other researchers. The (nondimensional) time increment is 0.005 such that the CFL number is lower than 0.5. Five subcyclings are used for each time step. The simulation is carried out up to 100 time units, when well developed vortex appears.

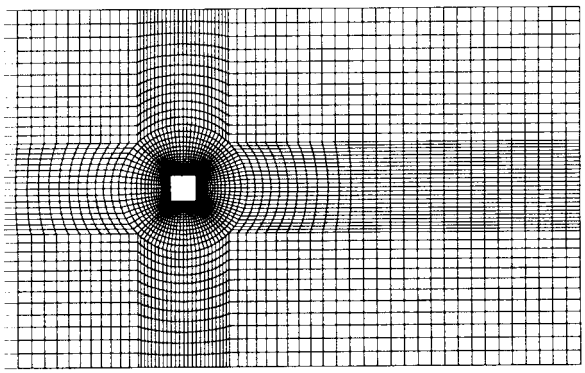

Fig. 2 Mesh distribution

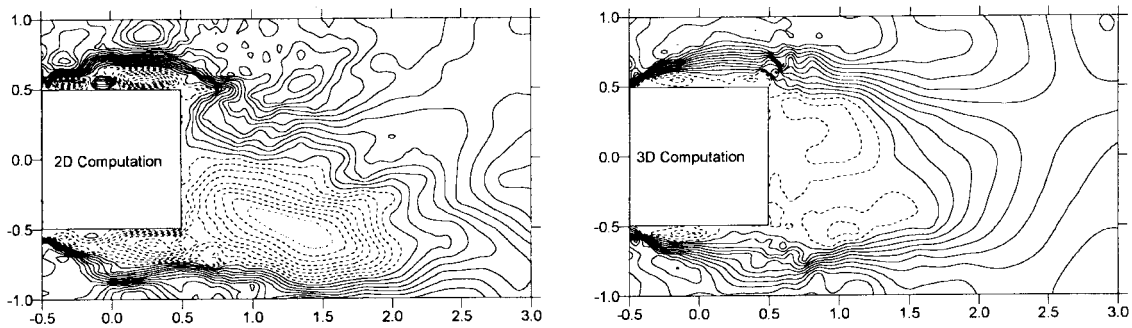

Fig. 3 Instantaneous streamwise velocity

Calculations for additional 100 time units (corresponding to approximately 13 shedding periods) are performed and the results are used to calculate statistical characteristics of the unsteady flow. A 3D computation of flow at Re=22000 required about 35 hours of user time on Cray Y-MP8/864.

Fig. 3 through 5 display the contour plots of the streamwise and vertical velocities and the spanwise vorticity near the cylinder in the *x-y* plane at an instant. In 3D case, the quantities are averaged in spanwise direction. Each figure compares the results from 2D and 3D computations. The comparisons are made at the instant when the lift coefficient is near its maximum and starts to decrease. In the case of 2D, the formation of vortices on the side walls and the strong vortex near the leeward face are clearly seen. The shear layers which separated at the windward corners are distorted by the strong vortex motion near the side walls of the cylinder. The distorted shear layers lead to the broad width of the wake which is responsible for the increase of drag. The concentrations of strong vortices on the surface of the cylinder for the two-dimensional case are obviously shown in Fig. 5 where the spanwise vorticity contours are compared. Large scale vortex motions found very close to the surface of the cylinder lead to large fluctuating forces acting on the cylinder with the narrow-banded power spectra. It is often postulated that the formation of the strong vortices is due to the lack of the effects of three-dimensional diffusion and the vortex stretching mechanism. This is in accordance with the results of Tamura (1990). On the other hand, 3D results exhibit the separated shear layers which flow downward along the side walls without any distinct distortion. Both the streamwise and vertical velocity fields, and the resulting vorticity field show smooth variation in space, whereas rapid changes of those quantities are observed in 2D case. The strength of the vortices adjacent to the side walls from 3D

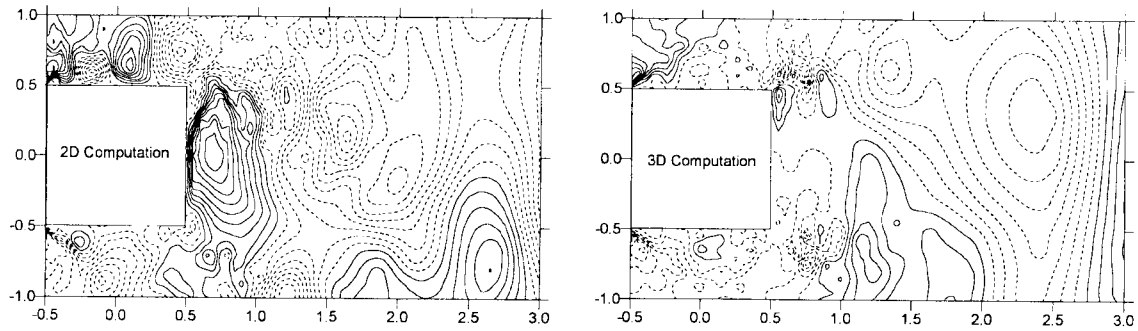

Fig. 4 Instantaneous vertical velocity

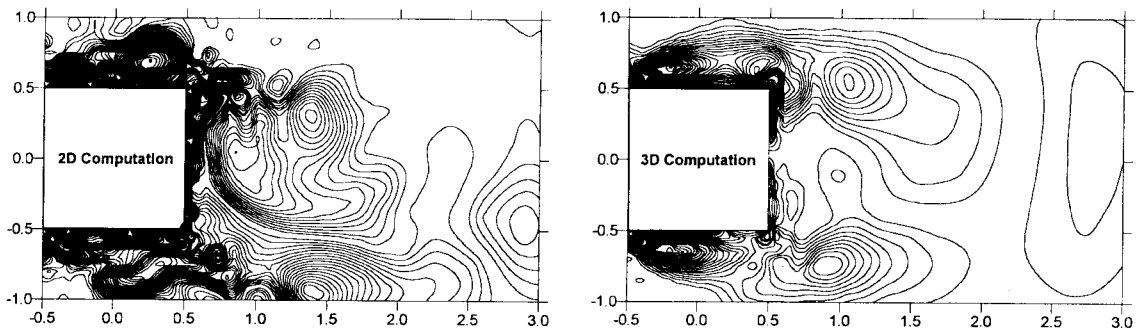

Fig. 5 Instantaneous spanwise vorticity

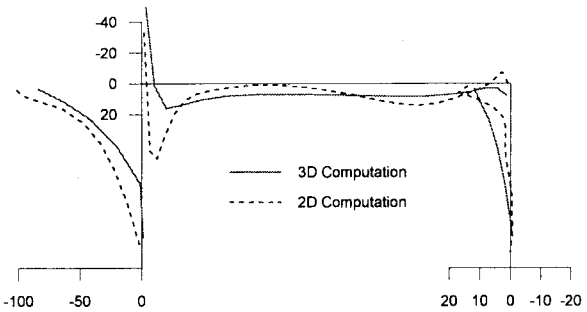

Fig. 6 Time-averaged spanwise vorticity on cylinder surface

computation is weaker than that of 2D calculation due to 3D mechanism described above.

Fig. 6 presents a comparison of time-averaged spanwise vorticity distributions along the surface of the cylinder. In the case of 3D computation an averaging is performed in the spanwise direction. The other components of the vorticity vector are very small compared to the spanwise component. The strength of vorticity of 2D simulation is in general larger than that in 3D computation. This is in accordance with the observations made for the instantaneous quantities. In particular, rapid change of vorticity in the 2D computation is seen, and the possibility of reattachment and detachment is clearly shown, while 3D simulation reproduced a rather smooth variation of vorticity on all sides.

Fig. 7 shows the distribution of RMS of the fluctuating component of pressure. The lowest RMS is at the stagnation point on the windward face, while higher values appear on the side wall. The fluctuation decreases as the center line of the leeward face is approached. The present results are compared with the experimental data of Bearman (1982). Apparently, the departure of the result of 2D computation from the expected value is large, and even the trend along the surface is different. The unusual deviation of RMS of fluctuating pressure from the expected value observed near the windward corners seems persistent regardless of the dimensionality, even though 3D computation shows improvement. A possible explanation for this phenomenon can be found in a study by Murakami (1996). The study pointed out that the Smagorinsky SGS model overestimates eddy viscosity near the windward corners due to

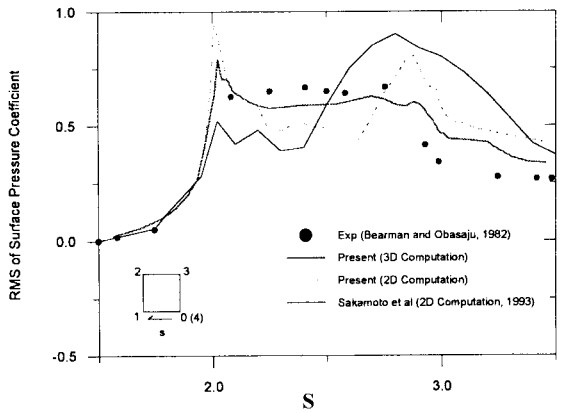

Fig. 7 RMS of fluctuating pressure on cylinder surface

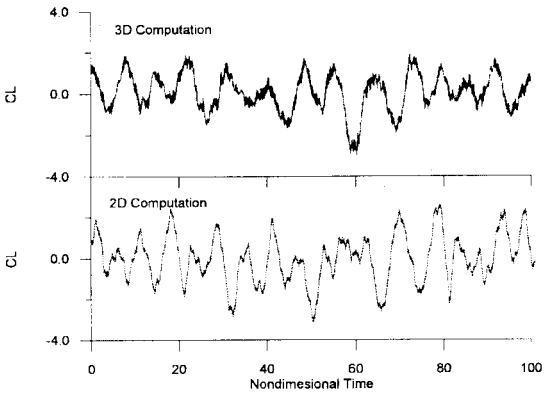

Fig. 8 Time histories of lift coefficient

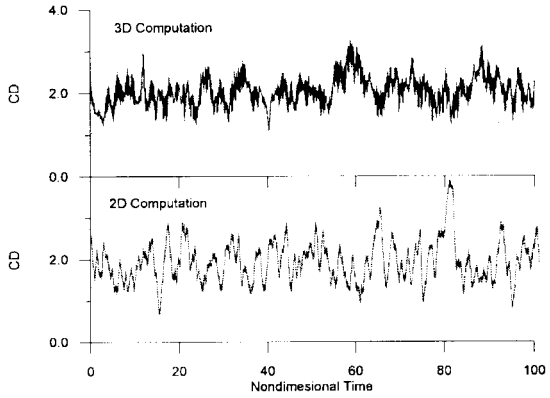

Fig. 9 Time histories of drag coefficient

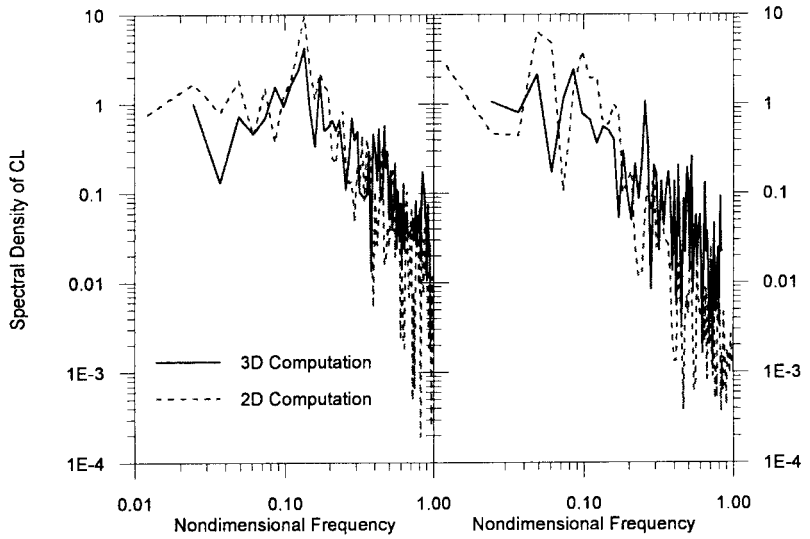

Fig. 10 Power spectra of lift and drag coefficients

the large mean strain, which is essentially one of the drawbacks of the model.

It was numerically shown by Lee (1997) that the forces acting on the body surface are highly correlated with ambient flow field. Figs. 8 and 9 compare the time histories of drag and lift coefficients, in which the forces simulated by 3D simulation exhibit predominant large structures corresponding to the primary shedding frequency. They also reveal highly fluctuating components, possibly contributed by small scale structures. However, the cause of the occurrence of the fluctuating components with extremely high frequency is unclear at present. A similar conclusion can be drawn by considering the power spectra shown in Fig. 10. The 3D computation produces such spectral distributions that energy is distributed over a wide range of frequency, illustrating the vortex stretching mechanism and the process of energy cascade. As a result, the power spectra of both lift and drag of the three-dimensional simulation tend to be broader than those of 2D calculation. As for the peak values in the spectra, 3D simulation reproduces smaller values than those of 2D calculation. This is consistent with the characteristics of the instantaneous flow field

Table 1 Comparison of integral parameters of 3D calculations

Computational Cases			Re	St	C_D		$(C_L)_{rms}$	l_r
					Mean	rms		
Present	2D LES	FEM (4776)	22000	0.134	2.15	0.74	1.6	0.80
	3D LES (SM)	FEM (47760)	22000	0.134	2.06	0.33	1.214	0.75
Franke and Rodi (1993)	2D RSE (wall function)	FVM (4480)	22000	0.136	2.15	-	-	0.47
Murakami and Mochida (1995)	3D LES (SM)	FDM (71760)	22000	0.132	2.09	-	-	0.64
Yu and Kareem (1996)	3D LES (SM)	FDM	100000	0.135	2.14	0.25	1.15	0.91

Experimental	Blockage (%)	Aspect Ratio of Medel	Turbulence Intensity of Free stream (%)	Re	St	$(C_D)_{mean}$	$(C_L)_{rms}$	l_r
Lyn *et al.* (1994, 1995)	7	9.75	2-3	21400	0.132 - 0.134	2.1		0.88
Durao *et al.* (1988)	13	6	6	14000	0.13			
Okajima (1982)	1-17.5	13.3-100	0.5	20000	0.13			
Bearman and Obasaju (1982)	-		0.04	20000	0.13		1.2	

(..) Number of Elements of Nodes, l_r=time-averaged recirculation length measured from the leeward face of the cylinder St : estimated from the peak of the power spectrum of the lift coefficient

discussed earlier. The magnitude of the fluctuation measured by RMS of unsteady quantity is larger in 2D case than in 3D case. RMSs of the fluctuating components of lift and drag are 1.6 and 0.74 in 2D calculation, whereas 1.2 and 0.33 are predicted in 3D computation. The narrow spectra with large magnitude for the two-dimensional calculation are expected from the previous discussions.

The time-averaged quantities associated with the forces acting on the cylinder and the Strouhal numbers are compiled in Table 1. Both 2D and 3D computations result in 0.134 as the Strouhal numbers found at the frequency where the peak of the spectral distribution of lift coefficient is located. It is close to the experimental value of 0.13 measured by Okajima (1982). The drag coefficients computed by 2D and 3D computations are 2.15 and 2.06, respectively, and the time-averaged lift coefficient predicted is $O(10^{-2})$ in both computations. These results are in good agreement with other experimental and computational data.

These differences between 2D and 3D simulation results indicate that 3D structures strongly influence the near-wake at the Reynolds number of 22,000. Even though 2D calculation is capable of predicting the time-averaged quantities of lift and drag with reasonable accuracy, it is

not feasible to employ 2D simulation to predict unsteady characteristics of turbulent flow at this Reynolds number.

4. 3D wake structure behind a square cylinder

The wake structures behind the square cylinder resulting from 3D simulation are shown in Fig. 11 through 13, in which instantaneous contours of velocity components at three different locations downstream of the cylinder are depicted. Note that the locations are measured from the center of the cylinder. It appears that the lateral dimension of a shed vortex is approximately of the size of the cylinder. Propagation of the streamwise velocity is clearly shown in Fig. 11. The large region of negative velocity indicates the recirculation region, while two strips with steep gradient of the velocity above and below the cylinder illustrate the shear layers. As the location of x/H=3 is approached, most of the flow structures of small scale have diminished. Apparently

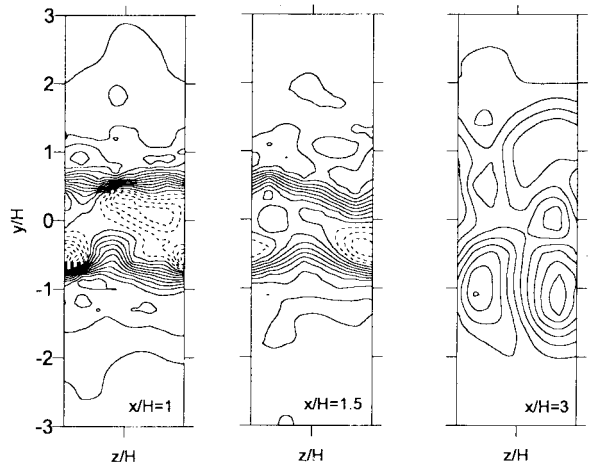

Fig. 11 Instantaneous streamwise velocity downstream of cylinder

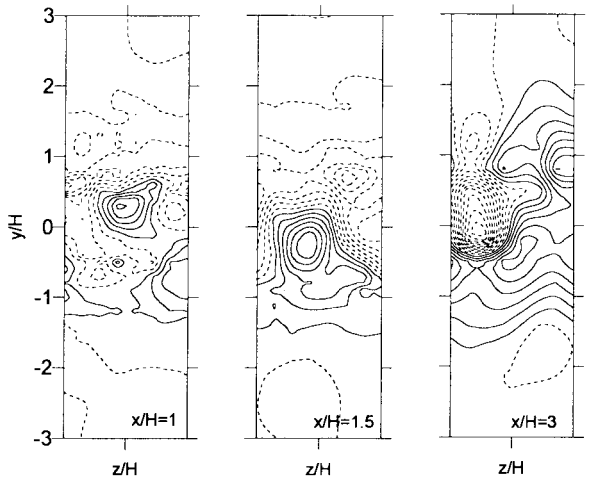

Fig. 12 Instantaneous vertical velocity downstream of cylinder

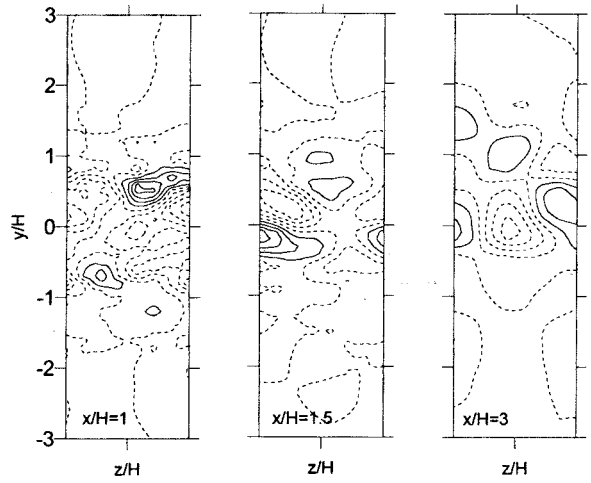

Fig. 13 Instantaneous lateral velocity downstream of cylinder

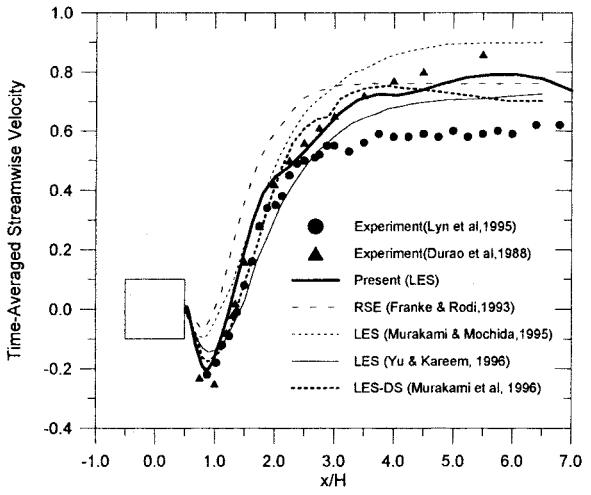

Fig. 14 Time-averaged streamwise velocity (U) along wake centerline downstream of cylinder

the distribution of the flow variables in the spanwise direction is highly non-uniform. Fig. 13 clearly shows the existence of the vorticity component in the flow direction (x), which is impossible to model in 2D computations.

The time-averaged (mean) streamwise (x-direction) velocity along the wake centerline is compared in Fig. 14 with the experimental data of Lyn (1995) and Durao (1988) and with the computational results reported by other researchers. Note that spanwise averaging is carried out for most of the results presented here unless otherwise specified. The discrepancy among the computational data may be attributed to differences in the numerical methods, the boundary conditions, and the computational parameters. The present method reproduces the mean velocity distributions fairly close to the experimental data, with a slightly shorter recirculation length. In most computational cases the recovery of velocity in the wake region ($x/H>3$) shows a relatively large departure from the experimental results reported by Lyn (1995). RMSs of the total (periodic+stochastic) fluctuations of the streamwise (U) and vertical (V)

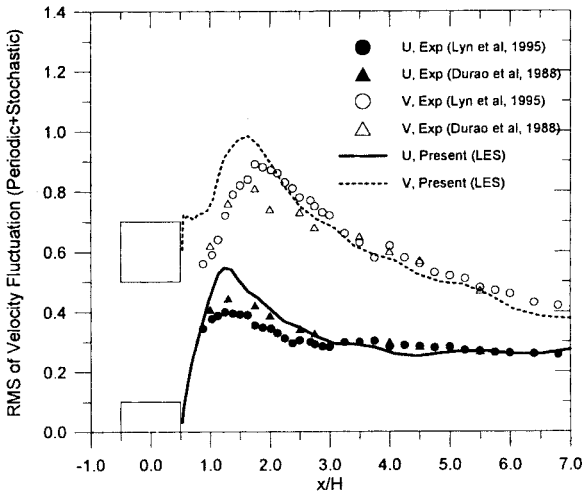

Fig. 15 RMS of velocity along wake centerline downstream of cylinder

velocity components are compared with the experimental data in Fig. 15. Both components are reasonably reproduced by the present calculations, except for the region very close to the cylinder. It is postulated that the simulated RMS of large magnitude near the cylinder is attributable to the aspect ratio of 2 and the relatively coarse grids in the spanwise direction employed in the present computation, because these affected the results such that the characteristics of the two-dimensionality are retained.

Fig. 16 compares the profiles of the computed and experimental velocity components, their RMSs and shear stresses at a location 0.5 H downstream of the leeward face of the cylinder. The present results are compared with only experimental data because no other computational data can be found in literature. The slight overestimation of the time-averaged streamwise velocity component near the centerline is consistent with the shorter mean recirculating zone

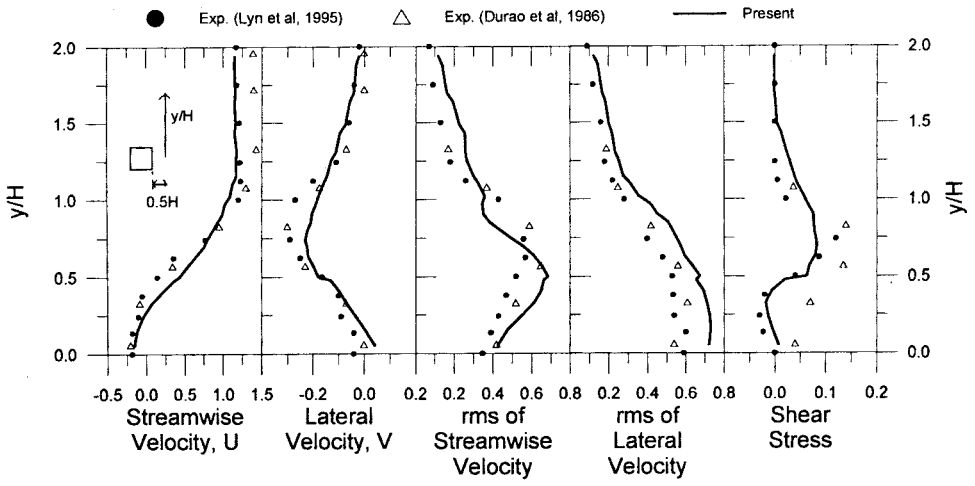

Fig. 16 Time-averaged profiles of velocities, RMS and shear stress at x/H=1 downstream of cylinder

of the predicted flow. This also leads to fast recovery of the streamwise velocity in the wake region, Fig. 14. The profiles of the averaged flow velocities indicate that the width of the computed wake is narrower than the experimental value. However, it is believed that the difference is not significant, considering that the difference in the drag coefficients between the present result and the experiment is very small. The profiles of computed RMSs of the fluctuating velocity show larger departures from the experimental values than those of the mean profiles. RMS of the vertical velocity is overestimated over the entire range of comparison, whereas RMS of the streamwise velocity is shifted toward the centerline. The peak of RMS of the streamwise velocity occurred approximately at the height of the cylinder, which indicates the strong activity of the vortex at that height. For the mean and RMS values, the comparisons between the present results and the experimental data show good agreement. In the Reynolds averaging sense of the turbulent shear stress, a correlation of fluctuating components of velocity is calculated. In the figure, u' and v' denote total fluctuating component of streamwise and vertical velocities, respectively. The profile exhibits two extrema : one in the shear layer and the other in the recirculation zone, which were also observed experimentally by Lyn (1995).

Since the flow of interest has noticeable coherent structures associated with vortex shedding, the concept of phase averaging is introduced to extract the turbulent components from the total unsteady quantity, Hussain (1983). Phase averaging leads to decomposition of the flow variables into time-averaged (mean), periodic (coherent) and stochastic (turbulent) components. Figs. 17 through 19 display an instantaneous velocity field, the corresponding phase-averaged velocity field, and the stochastic velocity field, respectively. Note that the vector plots in Fig. 19 are exaggerated for clarity. Fig. 17 shows vortex structures of wide range in size developed around and behind the cylinder. The phase-averaged velocity field in Fig. 18 retains the large structures of vortices, whereas fine structures are filtered out through phase averaging. On the other hand, the extracted stochastic components of velocity field in Fig. 19 show that small scales of vortices close to the cylinder are generated by the incoherent structures. These characteristics can not be discovered if a conventional time-averaging is employed. Instead, the phase-averaging is capable of identifying distinct features of the coherent and the stochastic structures.

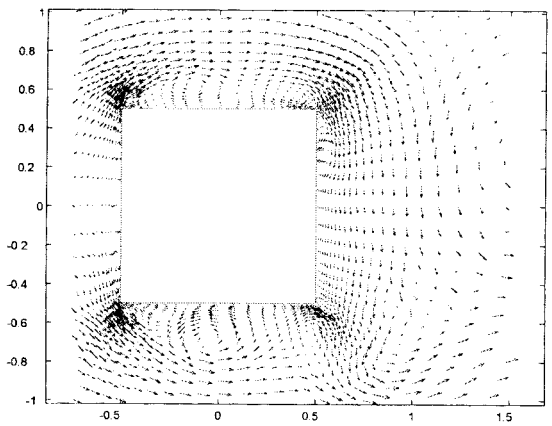

Fig. 17 Instantaneous velocity field

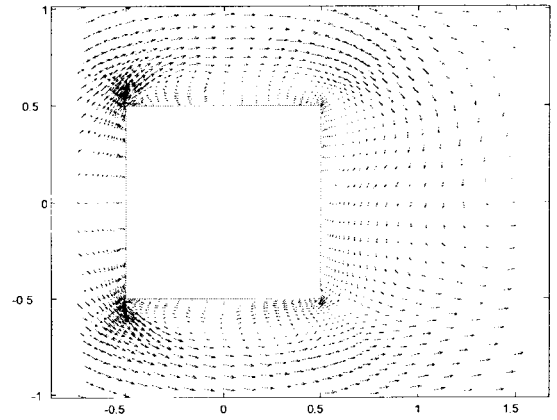

Fig. 18 Phase-averaged velocity field

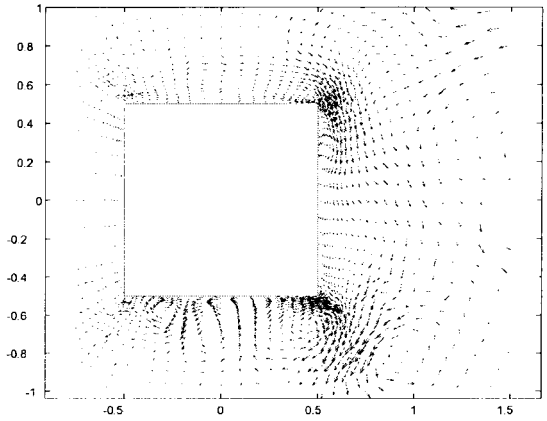

Fig. 19 Instantaneous stochastic velocity field

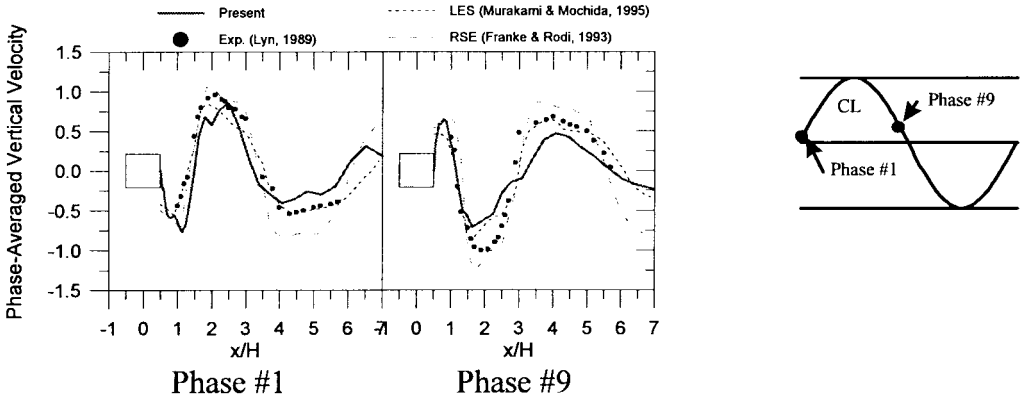

Fig. 20 Phase-averaged vertical velocity (V) along certer downstream for two representative phase

Fig. 20 show the phase averaged vertical velocity distributions along the wake centerline downstream of cylinder for two representative phases. The definitions of Phases #1 and #9 are depicted in a small diagram. The present results near the cylinder are in good agreement with the experimental data of Lyn (1989) as well as with the other computational results. However, the magnitude of the computed vertical velocity decreases faster than the experimental value. In order to identify the numerical mechanism responsible for the reduced magnitude of the phase averaged vertical velocity along the wake centerline, the SGS eddy viscosity and the artificial viscosity induced by the streamline upwind scheme were compared. Since the artificial viscosity in the upwind scheme has the form of tensor, its determinant was computed. The comparison shows that the SGS eddy viscosity has approximately same order of magnitude as the molecular viscosity except for the region very close to the cylinder, whereas the artificial viscosity is at least one order smaller than others. This indicates a large dissipation that is deemed to be attributable to high eddy viscosity occurring away from the cylinder due to relatively coarse mesh in that region.

Figs. 21a through 21e show a time sequence of streaklines past the square cylinder. A streakline is the trace of a series of particles released at a certain position at the entrance of the domain. In

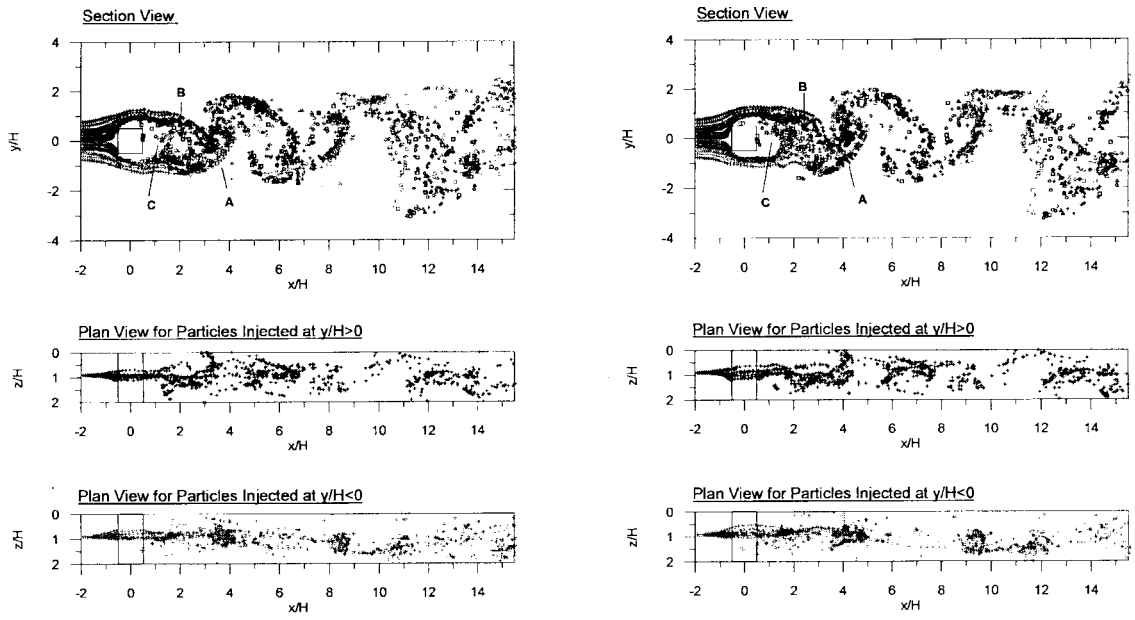

(a) Frame 1 (b) Frame 2

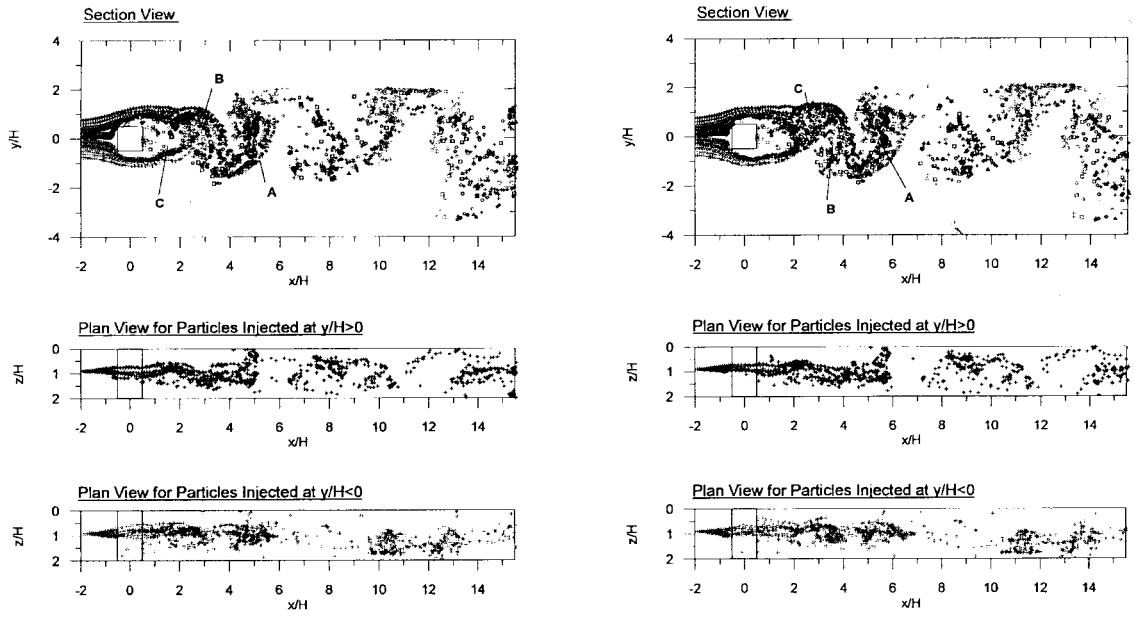

(c) Frame 3 (d) Frame 4

Fig. 21(a) Streaklines

the present computation, massless particles are injected into the domain along a vertical line 2H ahead of the cylinder at each time step. The trajectory of the particle is computed using three-dimensional velocity so that three-dimensional vortices can be visualized. Five frames of the streakline plots are presented, and each frame corresponds to the instance defined in Fig. 21f.

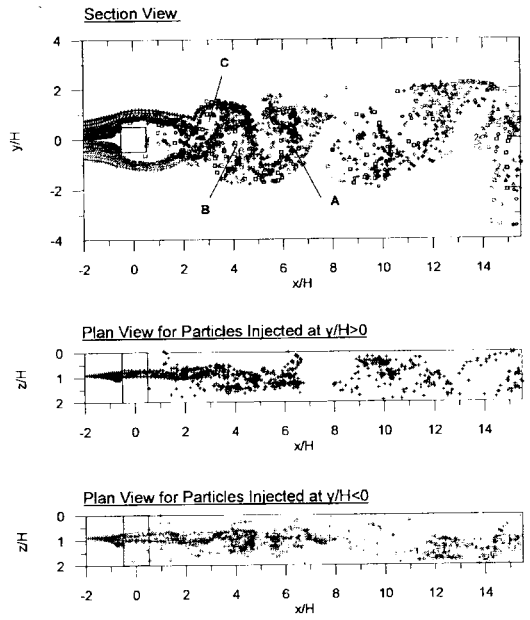

(e) Frame 5

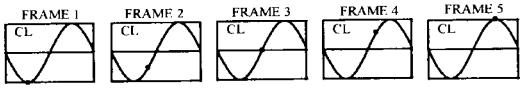

(f) Definition of Frames

Fig. 21(b) Streaklines

Each figure includes not only a sectional view in the *x-y* plane but also plan views in the *x-z* plane so that the three-dimensional structure of a vortex can be identified. In addition, the plan views are plotted separately for the particles injected at $y/H>0$ and at $y/H<0$. The streaklines clearly illustrate continuous formation and shedding mechanism of the vortices. Combined views of the *x-y* and *x-z* planes well visualize three-dimensional coherent structures. The coherent masses in three-dimensional space developed behind the cylinder are convected downstream and finally start to spread out far downstream due to the diffusive nature of turbulence.

5. Conclusions

2D and 3D turbulent flows past a square cylinder at Re=22,000 are numerically simulated using LES implemented with FEM, and unsteady flow characteristics of the flow have been studied in this chapter.

2D computation reproduces relatively strong vortices close to the cylinder. This affected the pressure field on the surface of the cylinder, leading to the power spectra of the force coefficients with narrow band width. The separated shear layers are also distorted by the strong activities in the vicinity of the cylinder. Although mean quantities of drag and lift are predicted close to the experimental values, RMSs of fluctuating forces are overestimated due to the nearby strong vortices. In particular, the distribution of RMS of fluctuating pressure on the surface of the cylinder showed a large departure from the expected values.

The results of 3D simulation are found to be in a good agreement with both experimental and computational data reported by other researchers. Time-averaged quantities as well as RMS values of fluctuating components of drag and lift are well predicted. The computed power spectra

of force coefficients clearly showed the three-dimensional effects of the vortex stretching mechanism and corresponding energy cascade.

Wake structures in the vortex-shedding flow field behind a square cylinder are well reproduced by the present method. Time-averaged streamwise velocity and kinetic energy distributions downstream of the cylinder are in good agreement with the compared data. Fluctuating components of the simulated velocity adjacent to the surface of the cylinder are overestimated but showed in general good agreement with the experimental values. The time-averaged recirculation length is found to be slightly shorter than the expected value inferred from the experimental data. In addition, a fast recovery of the velocity field beyond the recirculation region is observed. Phase-averaged velocities downstream of the cylinder also agree well with the compared data. Time-averaged profiles downstream of the cylinder also agree well with the experimental data. They show that the present approach can reproduce not only mean velocities and auto-correlated quantities (RMS) but also cross-correlated values (shear stress) in the wake structures. The mechanism of vortex shedding is well identified by the numerical flow visualization of streaklines.

References

Brooks, A., and J.R. Hughes, (1982) "Streamline upwind/Petrov-Galerkin formulations for convection dominated flows with particular emphasis on incompressible Navier-Stokes equations", *Comp. Methods in App. Mech. Eng.*, **32**, 199-259.

Bearman, P.W., and E.D. Obasaju, (1982) "An experimental study of pressure fluctuations on fixed and oscillating square-section cylinders", *J. Fluid Mech.*, **119**, 297-321.

Durao, D.F.G., M.V. Heitor, and J.C. Pereira, (1988), "Measurements of turbulent and periodic flows around a square cross-section cylinder", *Exp. Fluids*, **6**, 298-304.

Franke, R., W. Rodi, and B. Schonung, (1990), "Numerical calculation of laminar vortex shedding flow past cylinders", *J. Wind Eng. & Ind. Aerodyn.*, **35**, 1990, 237-257.

Franke, R., and W. Rodi, (1993), "Calculation of vortex shedding past a square cylinder with various turbulent models", *Turbulent Shear Flows VIII*, 189-204.

Gresho, P.M., S.T. Chan, R.L. Lee, and C.D. Upson, (1984), "A modified finite element method for solving the time-dependent, incompressible Navier-Stokes equations. Part 1 : Theory", *Int. J. Num. Methods in Fluids*, **4**, 557-598.

Hussain, A.K.M.F., (1983), "Coherent structures-reality and myth", *Phys Fluids*, **26**, (10), Oct., 2816-2850.

Lee, S., and B. Bienkiewicz, (1998), "Finite element implementation of large eddy simulation for separated flows", *J. Wind Engr. & Ind. Aerodyn.* (in print).

Lee, S., (1997) Large eddy simulation of flow past a square cylinder using finite element method, Ph.D Dissertation, Colorado State University, Ft. Collins, USA.

Lyn, D.A., (1989), "Phase-averaged turbulence measurements in the separated shear layer region of flow around a square cylinder", *Proc. 23rd Cong. Int. Ass. Hydraulic Res.*, Ottawa, Canada, **A**, 85-92.

Lyn, D.A., W. Rodi, (1994), "The flapping shear layer formed by flow separation from the forward corner of a square cylinder", *J. Fluid Mech.*, **267**, 353-376.

Lyn, D.A., and E. Einav, W. Rodi, and J.-H. Park, (1995), "A laser-Doppler velocimeter study of ensemble-averaged characteristics of the turbulent near wake of a square cylinder", *J. Fluid Mech.*, **304**, 285-319.

Murakami, S., A. Mochida and K. Hibi, (1987), "Three-dimensional numerical simulation of air flow around a cubic model by means of large eddy simulation", *J. Wind Eng. Ind. Aerodyn.*, **25**, 1997, 291-305.

Murakami, S., A. Mochida, and S. Iizuka, (1996) "New trends in turbulence models for prediction of wind effects on structures", *IWEF Workshop on CWE/CFD for Pred. Wind Effects on Structures, Aug.*

Murakami, S., and A. Mochida, (1995), "On turbulent vortex shedding flow past 2D square cylinder predicted by CFD", *J. Wind Engr. & Ind. Aerodyn.*, **54/55**, 191-211.

Nomura, T., and M. Jiravacharadet, (1995), "Finite element analysis of turbulent flows around a circular cylinder using the Smagorinsky model", *IWEF Workshop on CFD for Pred. Wind Load. on Buildings and Structures*, Tokyo, Japan, Sep.

Okajima, A., (1982), "Strouhal numbers of rectangular cylinders", *J. Fiuid Mech.,* **123**, 379-398.

Roshko, (1993), "Perspectives on bluff body aerodynamics", *J. Wind Engr. & Ind. Aerodyn.*, **49**, 79-100.

Sakamoto, S., S. Murakami, S. Kato, and A. Mochida, "Unsteady pressure field around oscillating prism predicted by LES", *J. Wind Engr. & Ind. Aerodyn.*, **46/47**, 551-556.

Smagorinsky, T.S., (1963), "General circulation experiment with primitive equations : Part I, Basic experiments", *Monthly Weather Review*, **91**, 99-164.

Tamura, T. and K. Kuwahara, (1990), "Numerical study of aerodynamic behavior of a square cylinder", *J. Wind Engr. & Ind. Aerodyn.*, **33**, 161-170.

Yu, D.-H., and A. Kareem, (1996), "Numerical simulation of flow around rectangular prism", *2nd Int. Conf. Comp. Wind Engr.*, Ft. Collins, USA, Aug.